Mercury's Magnetosphere After MESSENGER's First Flyby

James A. Slavin, *et al.*

Science **321**, 85 (2008);
DOI: 10.1126/science.1159040

in the plasma pressure of ~1.8 nPa. Also, coincident with the drop in field magnitude at C, the plasma proton count rates increased by a factor of three (*18*). The change in magnetic field magnitude implies a plasma pressure increase at C of ~2 nPa. Because the proton count rates before C were ~30% of those after C, the pressure before C was ~1 nPa, which would depress the field by ~7 nT.

Such signatures are consistent with hybrid simulations of Mercury's magnetosphere (*19*) that indicate an annulus of solar wind plasma within ~0.5 R_M altitude. The inward pressure gradient at the outer edge of such an annulus would suppress the magnetic field near the equator on the nightside and enhance it over the poles. The corresponding westward azimuthal current is about $I = hP/B$, where h is the vertical extent of the annulus, B is the magnetic field magnitude, P is the pressure in the annulus, and the pressure outside is taken to be zero. A 1-nPa pressure that goes to zero near 0.5 R_M altitude, where the field is ~50 nT, and that has a vertical extent of ~0.5 R_M corresponds to a current of 0.05 to 0.1 MA. This would decrease the equatorial field close to the planet by 10 to 30 nT and increase the field at the pole by ~5 to 10 nT. Thus, it is possible that the remaining deficit of equatorial field intensity of ~25 nT could be due to magnetospheric plasma. We conclude that an intrinsic quadrupole term is not required to account for the observations.

Recent simulations of Mercury's core dynamo suggest that the presence of a stagnant layer at the top of the molten outer core may suppress higher-order structure and yield secular variation over time scales of centuries rather than decades (*20*–*22*). We find no evidence for a change in the planetary dipole since 1974 and also find that the planetary field is predominantly and possibly entirely dipolar. Although there are significant uncertainties associated with these results, they are consistent with the presence of a stagnant outermost core.

References and Notes

1. N. F. Ness, K. W. Behannon, R. P. Lepping, Y. C. Whang, K. H. Schatten, *Science* **185**, 151 (1974).
2. N. F. Ness *et al.*, *J. Geophys. Res.* **80**, 2708 (1975).
3. N. F. Ness *et al.*, *Icarus* **28**, 479 (1976).
4. S. C. Solomon, *Icarus* **28**, 509 (1976).
5. L. J. Srnka, *Phys. Earth Planet. Inter.* **11**, 184 (1976).
6. D. J. Jackson, D. B. Beard, *J. Geophys. Res.* **82**, 2828 (1977).
7. J. E. P. Connerney, N. F. Ness, in *Mercury*, F. Vilas, C. R. Chapman, M. S. Matthews, Eds. (Univ. of Arizona Press, Tucson, 1988), pp. 494–513.
8. S. C. Solomon *et al.*, *Science* **321**, 59 (2008).
9. B. J. Anderson *et al.*, *Space Sci. Rev.* **131**, 417 (2007).
10. J. A. Slavin *et al.*, *Science* **321**, 85 (2008).
11. J. G. Luhmann *et al.*, *J. Geophys. Res.* **103**, 9113 (1998).
12. H. Korth *et al.*, *Planet. Space Sci.* **52**, 733 (2004).
13. N. A. Tsyganenko, M. I. Sitnov, *J. Geophys. Res.* **110**, A03208, 10.1029/2004JA010798 (2005).
14. D. Winch, in *Encyclopedia of Geomagnetism and Paleomagnetism*, D. Gubbins, E. Herrero-Bervera, Eds. (Springer, Dordrecht, Netherlands, 2007), pp. 448–452.
15. R. L. Parker, *Geophysical Inverse Theory* (Princeton Univ. Press, Princeton, NJ, 1994).
16. J. D. Bloxham *et al.*, *Philos. Trans. R. Soc. London Ser. A* **329**, 415 (1989).
17. C. J. Johnson, C. G. Constable, *Geophys. J. Int.* **122**, 489 (1995).
18. T. H. Zurbuchen *et al.*, *Science* **321**, 90 (2008).
19. P. Trávníček *et al.*, *Geophys. Res. Lett.* **34**, L05104, 10.1029/2006GL028518 (2007).
20. U. R. Christensen, *Nature* **444**, 1056 (2006).
21. F. Takahashi, M. Matsushima, *Geophys. Res. Lett.* **33**, L10202 10.1029/2006GL025792 (2006).
22. J. Wicht *et al.*, *Space Sci. Rev.* **132**, 261 (2007).

23. The MESSENGER project is supported by the NASA Discovery Program under contracts NAS5-97271 to Johns Hopkins University Applied Physics Laboratory and NASW-00002 to the Carnegie Institution of Washington. Support was also provided under the NASA MESSENGER Participating Science Program via grant NNX07AR73G.

14 April 2008; accepted 6 June 2008
10.1126/science.1159081

REPORT

Mercury's Magnetosphere After MESSENGER's First Flyby

James A. Slavin,[1]* Mario H. Acuña,[2] Brian J. Anderson,[3] Daniel N. Baker,[4] Mehdi Benna,[2] George Gloeckler,[5,6] Robert E. Gold,[3] George C. Ho,[3] Rosemary M. Killen,[6] Haje Korth,[3] Stamatios M. Krimigis,[3,7] Ralph L. McNutt Jr.,[3] Larry R. Nittler,[8] Jim M. Raines,[5] David Schriver,[9] Sean C. Solomon,[8] Richard D. Starr,[10] Pavel Trávníček,[11] Thomas H. Zurbuchen[5]

Observations by MESSENGER show that Mercury's magnetosphere is immersed in a comet-like cloud of planetary ions. The most abundant, Na^+, is broadly distributed but exhibits flux maxima in the magnetosheath, where the local plasma flow speed is high, and near the spacecraft's closest approach, where atmospheric density should peak. The magnetic field showed reconnection signatures in the form of flux transfer events, azimuthal rotations consistent with Kelvin-Helmholtz waves along the magnetopause, and extensive ultralow-frequency wave activity. Two outbound current sheet boundaries were observed, across which the magnetic field decreased in a manner suggestive of a double magnetopause. The separation of these current layers, comparable to the gyro-radius of a Na^+ pickup ion entering the magnetosphere after being accelerated in the magnetosheath, may indicate a planetary ion boundary layer.

The interaction of Mercury's magnetic field with the solar wind creates a small magnetosphere with a typical standoff altitude of ~0.5 R_M (where R_M is the mean planet radius; 1 R_M ~ 2440 km) (*1*, *2*) (Fig. 1). The MESSENGER spacecraft made the first of three flybys of Mercury on 14 January 2008 (*3*) and took measurements within Mercury's magnetosphere with its magnetometer (MAG) (*4*, *5*); energetic particle and plasma spectrometer, composed of the energetic particle spectrometer (EPS) and fast imaging plasma spectrometer (FIPS) (*6*, *7*); and x-ray spectrometer (XRS) (*8*).

The presence of the magnetosphere as an obstacle to the solar wind is signaled by the bow shock (BS), which was crossed at 18:08:38 (inbound) and 19:18:55 (outbound). Before the inbound magnetopause (MP) crossing at 18:43:02, the last extended interval of southward interplanetary magnetic field (IMF) ended at 18:38:40. The magnetosheath magnetic field was observed to be generally northward after the exit from the magnetosphere at 19:14:15. A northward IMF is unfavorable to dayside magnetic reconnection with Mercury's magnetic field and greatly limits the rate of solar wind energy transfer across the

[1]Heliophysics Science Division, NASA Goddard Space Flight Center, Greenbelt, MD 20771, USA. [2]Solar System Exploration Division, NASA Goddard Space Fight Center, Greenbelt, MD 20771, USA. [3]Johns Hopkins University Applied Physics Laboratory, Laurel, MD 20723, USA. [4]Laboratory for Atmospheric and Space Physics, University of Colorado, Boulder, CO 80303, USA. [5]Department of Atmospheric, Oceanic, and Space Sciences, University of Michigan, Ann Arbor, MI 48109, USA. [6]Department of Astronomy, University of Maryland, College Park, MD 20742, USA. [7]Academy of Athens, Athens 11527, Greece. [8]Department of Terrestrial Magnetism, Carnegie Institution of Washington, Washington, DC 20015, USA. [9]Institute of Geophysics and Planetary Physics, University of California, Los Angeles, CA 90024, USA. [10]Department of Physics, Catholic University of America, Washington, DC 20064, USA. [11]Astronomical Institute, Academy of Sciences of the Czech Republic, Prague, Czech Republic.

*To whom correspondence should be addressed. E-mail: james.a.slavin@nasa.gov

MP (*2*). The earlier southward IMF intervals before MESSENGER's entry into the magnetosphere were expected to produce strong energetic particle acceleration, as had been observed during Mariner 10's first flyby (*2*). The lack of measurable energetic electrons within the magnetosphere during MESSENGER's flyby (Fig. 2) indicates that energetic electrons remained within the magnetosphere for less than the ~4 min between the time when the southward IMF ended and when MESSENGER entered the magnetosphere.

MESSENGER observed a well-defined flux transfer event (FTE) between 18:36:21 and 18:36:25 during its passage through the magnetosheath (Fig. 2). FTEs are produced by localized magnetic reconnection between the IMF and the planetary magnetic field at the MP (*9*). The magnetic field data in Fig. 3A show that this FTE was indeed preceded by a brief interval of southward IMF. Its flux rope topology is apparent, with the helical magnetic field surrounding and supporting the core region indicated by the bipolar B_y signature and the strong B_z, respectively. Given a typical anti-sunward magnetosheath flow speed of ~300 km s^{-1} and the ~4-s duration of the event, the size of this FTE is ~1200 km or ~0.5 R_M. Relative to Mercury's magnetosphere, this FTE is ~10 times larger than the size found at Earth (*10*). This result supports predictions that finite gyro-radius effects in Mercury's small magnetosphere will lead to relatively large FTEs (*11*).

When MESSENGER passed into Mercury's magnetotail (Fig. 2), there was a rapid transition to a quieter magnetic field directed predominantly northward but with a longitude angle near 0°, indicating that the spacecraft entered through the dusk flank of the tail into the central plasma sheet (*12*). The dominance of the B_z component over B_x and B_y components and the sunward longitude angle indicate that MESSENGER passed just north of the center of the cross-tail current sheet (Fig. 1). The high ratio of thermal to magnetic pressure typical of this region (*12*) is evident from the weakness of the magnetic field intensity in Mercury's tail at this point relative to the adjacent magnetosheath.

Between 18:47 and 18:49, the longitude angle of the magnetic field rotated from 0° (i.e., sunward) to near 180° (anti-sunward). This change indicates that MESSENGER moved southward through the cross-tail current sheet, consistent with its trajectory in Fig. 1. Around 19:00, the spacecraft altitude fell below ~800 km, and the magnetic field intensity began to increase quickly as MESSENGER moved into the region dominated by Mercury's dipolar planetary magnetic field (*5*). The increase in the magnetic field continued through closest approach and then decreased until MESSENGER exited the magnetosphere near the dawn terminator.

Examination of the high-resolution magnetic field longitude angle in Fig. 3B shows one 360° and several 180° rotations of the magnetic field in the *X-Y* plane between 18:43 and 18:46. The durations of the rotations ranged from ~10 to 25 s. Such rotations of the magnetic field in Earth's tail near the interface between the flanks of the plasma sheet and the magnetosheath are thought to be caused by vortices driven by the Kelvin-Helmholtz

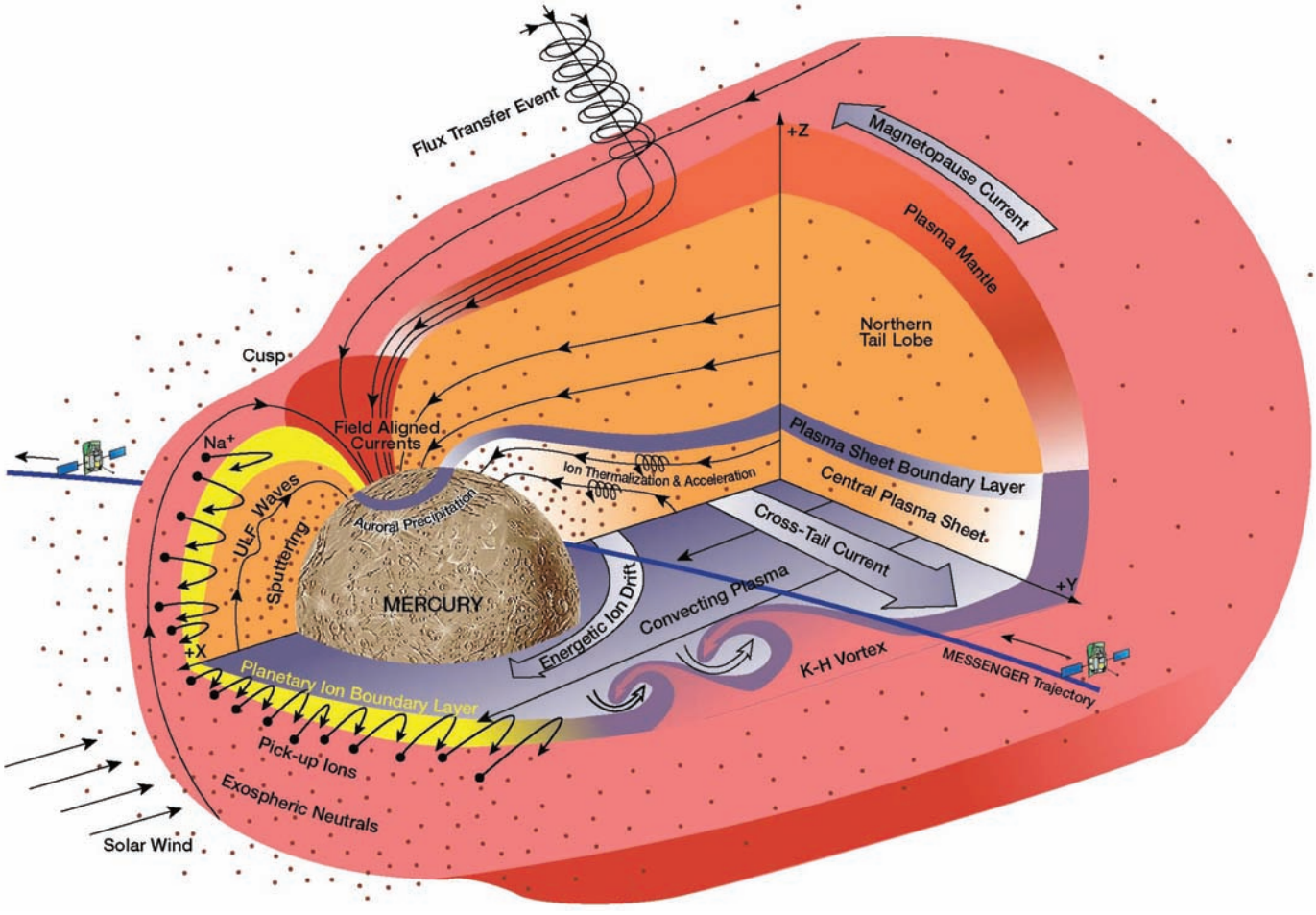

Fig. 1. Schematic of Mercury's magnetosphere highlighting the features and phenomena observed by MESSENGER, including the planetary ion boundary layer, large FTEs, flank K-H vortices, and ULF plasma waves.

(K-H) instability (*13*, *14*). Assuming Earth-like anti-sunward speeds of ~150 km s^{-1} (*14*) for these MESSENGER events, their implied spatial scale lengths are ~1 R_M. These scale lengths are smaller than similar features at Earth relative to the dimensions of their respective magnetospheres by a factor of ~3 (*14*).

The FIPS ion composition measurements show that Mercury's magnetosphere was permeated by planetary ions composed of Na^+ and other species in lesser amounts derived primarily from its exosphere (*15*). The coupling between these photoions and the magnetosphere has been the subject of extensive theory and modeling investigations (*16*–*20*) since sodium in Mercury's atmosphere was first detected telescopically from Earth (*21*). The spatial distribution of Na^+ (Fig. 2) represents a normalized count rate integrated over 3-min intervals (*7*). Further analysis is required to remove the effects of field-of-view obstructions and to determine bulk plasma properties such as density (*7*). The relative spatial distribution (Fig. 2) maximizes around closest approach, where the neutral atmosphere density should peak. This result is consistent with model predictions regarding the distribution of Na^+ within Mercury's magnetosphere (*17*). These models predict equatorial Na^+ densities along MESSENGER's near-tail trajectory that vary from 10^{-1} cm^{-3} to 10^{-2} cm^{-3} at dusk and dawn MPs, respectively (*17*). Secondary maxima in the FIPS Na^+ count rate exist just outside of the inbound and outbound MP crossings, indicating that the neutral sodium atmosphere extends to altitudes where photoions are strongly energized by pickup in the fast magnetosheath flow.

During the approach to Mercury, there were several intervals where the magnetic field decreased and its root mean square (RMS) variations increased (see horizontal bars in Fig. 2). Such variations are generally indicative of the growth of plasma waves stimulated by enhanced plasma density and/or temperature (*12*). The diamagnetic nature of these decreases is supported by the XRS count rates that increase around 19:00, coinciding with the first of these intervals (Fig. 2). The increase in XRS counts seen near 19:00 is believed to be due to fluorescence in the Mg- and Al-filtered

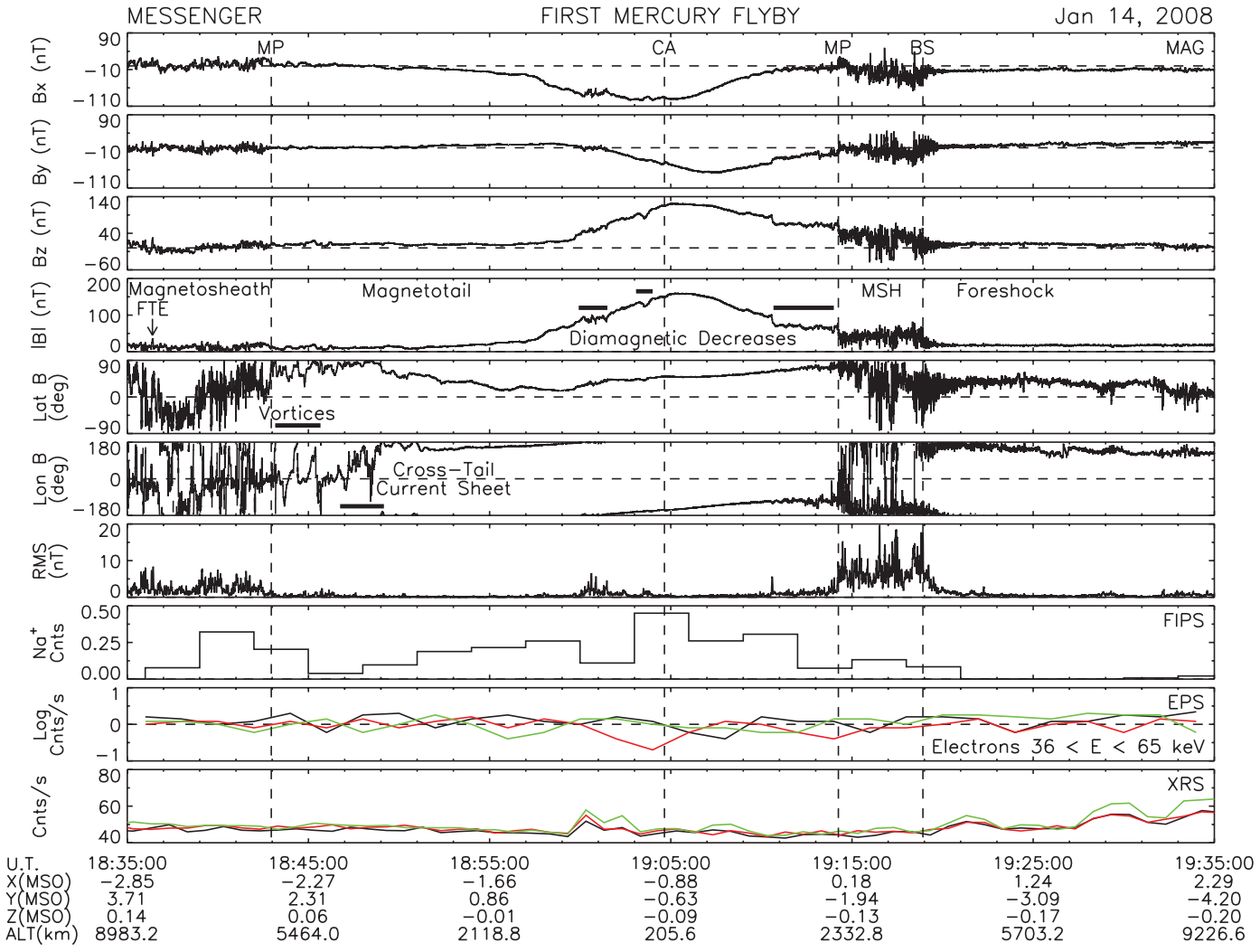

Fig. 2. Overview of MESSENGER magnetospheric measurements taken by the MAG, FIPS, EPS, and XRS instruments. Closest approach (CA) was at an altitude (ALT) of 201.4 km at 19:04:39 very near local midnight (00:04 local time). The magnetic field in Mercury solar orbital (MSO) coordinates is displayed in the top graphs along with the latitude and longitude direction angles and the RMS variance calculated over 3-s intervals. The MSO coordinate system is defined as X_{MSO} directed from the center of the planet toward the Sun; Z_{MSO}, normal to Mercury's orbital plane and positive toward the north celestial pole; and Y_{MSO}, positive in the direction opposite to orbital motion. The longitude angle of the magnetic field is defined to be 0° toward the Sun and increases counterclockwise looking down from the north celestial pole. The magnetic field latitude is +90° when directed northward and 0° when it is in the X_{MSO}-Y_{MSO} plane. U.T. designates universal time.

gas-proportional counters (GPCs) and to bremsstrahlung in both the Be window of the unfiltered GPC and the Be-Cu collimator in front of all three GPCs caused by electrons in the energy range ~1 to 10 keV. A similar response was seen in the GPCs on the Near-Earth Asteroid Rendezvous mission (*22*). The presence of enhanced fluxes of 1 to 10 keV electrons is consistent with these nightside diamagnetic decreases being due to the presence of hot plasma.

The strongest magnetic field decrease occurred after the narrow, MP-like current sheet encountered at 19:10:35. The orientation and thickness of this current sheet and the later MP current sheet are very similar, as can be inferred from the nearly identical variations in the magnetic field components (Fig. 4A). They differ primarily in intensity. The inner current sheet is only about half as strong as the MP current sheet. The difference in altitude between these two current sheets is ~1000 km. The enhanced RMS variations in the magnetic field indicate that the outer current sheet is the boundary between the magnetosphere and the magnetosheath and that the decreased magnetic field intensity between these two current sheets is due to enhanced plasma pressure [see also (*5*)].

This double MP signature had not been observed previously at Mercury or any other planetary magnetosphere. The decrease in the magnetic field in the outer part of the dawn-side magnetosphere may be caused by the diamagnetic effect of solar wind plasma flowing into the magnetosphere along flux tubes opened by reconnection near the cusps or locally created planetary ions. Although magnetic reconnection is expected to be more effective in creating open flux at Mercury than at other planets (*23*), it has not been observed elsewhere to produce such broad boundary layers or multiple current sheets. Alternatively, the inner current sheet and the diamagnetic layer could be caused by hot planetary ions that enter the magnetosphere after being picked up and accelerated by the fast solar wind flow in the magnetosheath. At the dawn terminator, the magnetosheath flow speed would typically be ~300 km s^{-1}. For Na^+, the depth of penetration into the magnetosphere would be ~1 gyro-radius or ~1000 km, a value comparable to the observed thickness of the region of depressed magnetic field. If present in sufficient numbers, pickup ions entering the magnetosphere from the magnetosheath might create a planetary ion boundary layer bounded by an inner current sheet and the MP (Fig. 1).

The pickup process produces ion distributions that are unstable to the growth of ion cyclotron waves and other plasma-wave modes (*24*–*26*). No clear wave trains near the Na^+ cyclotron frequency are present in the MESSENGER measurements, consistent with Mariner 10 observations (*27*). During its closest approach and outbound passage, however, MESSENGER did observe ultralow-frequency (ULF) waves with frequencies of ~0.5 to 1.5 Hz, or just

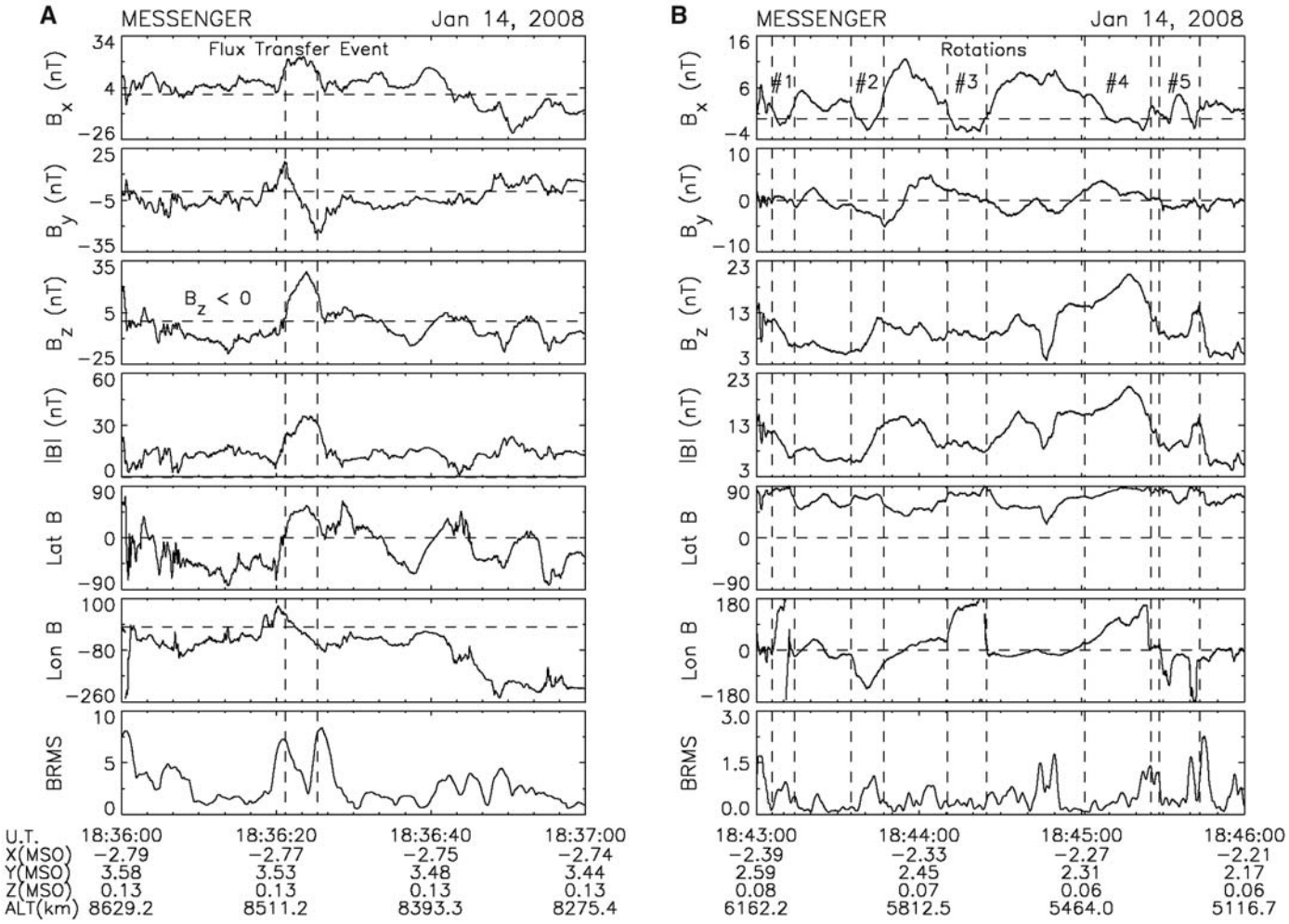

Fig. 3. (**A**) MESSENGER magnetic field observations of a large FTE in Mercury's magnetosheath. (**B**) Magnetic field observations of rotational signatures, possibly due to K-H–driven waves or vortices on the flanks of the magnetosphere.

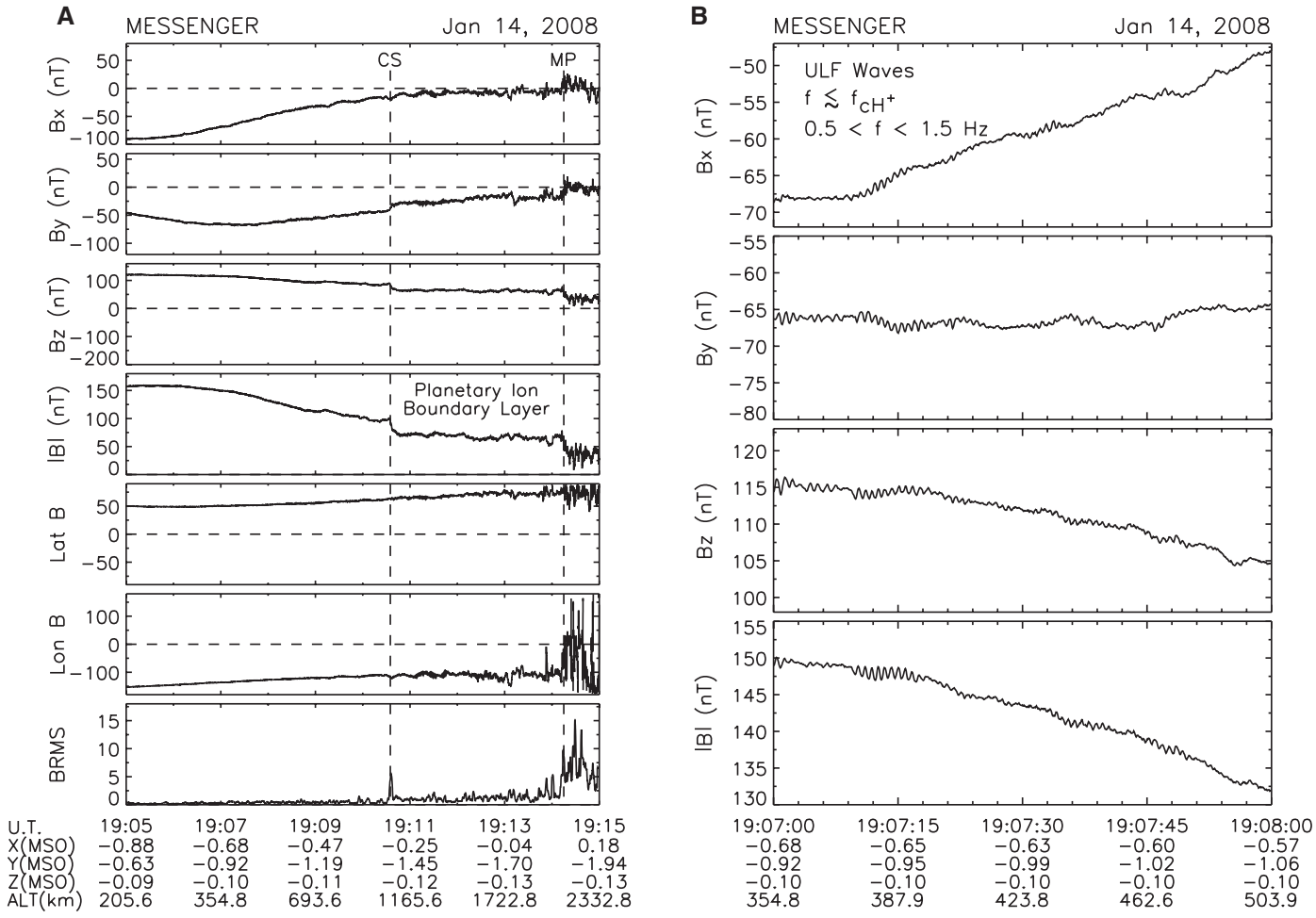

Fig. 4. (**A**) Magnetic field observations of the inner current sheet and MP boundary observed as MESSENGER exited the dawnside magnetosphere. (**B**) Magnetic field observations of ULF waves detected in Mercury's magnetosphere.

below the proton cyclotron frequency (f_{cH^+}) (Fig. 4B). They appear similar to the much shorter interval of ULF waves observed by Mariner 10 near closest approach during its first encounter (*28*). The frequency of these waves tended to increase with distance from Mercury until the outbound boundary layer was entered, where their frequency decreased and their amplitude increased to values as high as ~10 nT peak to peak.

MESSENGER has revealed Mercury's magnetosphere to be immersed in a cloud of cometlike planetary ions. Although the solar wind interaction appears dominated by Mercury's magnetic field, the presence of heavy planetary ions may exert influence from kinetic to magnetohydrodynamic scale lengths.

References and Notes

1. J. E. P. Connerney, N. F. Ness, in *Mercury*, F. Vilas, C. R. Chapman, M. S. Matthews, Eds. (Univ. of Arizona Press, Tucson, AZ, 1988), pp. 494–513.
2. C. T. Russell, D. N. Baker, J. A. Slavin, in *Mercury*, F. Vilas, C. R. Chapman, M. S. Matthews, Eds. (Univ. of Arizona Press, Tucson, AZ, 1988), pp. 514–561.
3. S. C. Solomon *et al.*, *Planet. Space Sci.* **49**, 1445 (2001).
4. B. J. Anderson *et al.*, *Space Sci. Rev.* **131**, 417 (2007).
5. B. J. Anderson *et al.*, *Science* **321**, 82 (2008).
6. G. B. Andrews *et al.*, *Space Sci. Rev.* **131**, 523 (2007).
7. T. H. Zurbuchen *et al.*, *Science* **321**, 90 (2008).
8. C. E. Schlemm *et al.*, *Space Sci. Rev.* **131**, 393 (2007).
9. C. T. Russell, R. C. Elphic, *Space Sci. Rev.* **22**, 681 (1978).
10. C. T. Russell, R. J. Walker, *J. Geophys. Res.* **90**, 11067 (1985).
11. M. M. Kuznetsova, L. M. Zeleny, in *Proceedings of the Joint Varenna-Abastumani International School and Workshop on Astrophysics*, Sponsoring Organization, Sukhumi, USSR, 19 to 28 May 1986 (European Space Agency SP-251, Noordwijk, Netherlands, 1986), pp. 137–146.
12. J. A. Slavin *et al.*, *J. Geophys. Res.* **90**, 10875 (1985).
13. D. H. Fairfield *et al.*, *J. Geophys. Res.* **105**, 21159 (2000).
14. M. Fujimoto *et al.*, *J. Geophys. Res.* **103**, 4391 (1998).
15. W. E. McClintock *et al.*, *Science* **321**, 92 (2008).
16. W.-H. Ip, *Icarus* **71**, 441 (1987).
17. D. C. Delcourt *et al.*, *Ann. Geophys.* **21**, 1723 (2003).
18. K. Kabin, T. I. Gombosi, D. L. DeZeeuw, K. G. Powell, *Icarus* **143**, 397 (2000).
19. E. Kallio, P. Janhunen, *Ann. Geophys.* **21**, 2133 (2003).
20. P. Trávníček, P. Hellinger, D. Schriver, *Geophys. Res. Lett.* **34**, L05104, 10.1029/2006GL028518 (2007).
21. A. Potter, T. Morgan, *Science* **229**, 651 (1985).
22. R. D. Starr *et al.*, *Adv. Space Res.* **24**, 1159 (1999).
23. J. A. Slavin, R. E. Holzer, *J. Geophys. Res.* **84**, 2076 (1979).
24. A. L. Brinca, B. T. Tsurutani, *Astron. Astrophys.* **187**, 311 (1987).
25. K.-H. Glassmeier, D. Klimushkin, C. Othmer, P. Mager, *Adv. Space Res.* **33**, 1875 (2004).
26. L. G. Blomberg, J. A. Cumnock, K.-H. Glassmeier, R. A. Treumann, *Space Sci. Rev.* **132**, 575 (2007).
27. S. A. Boardsen, J. A. Slavin, *Geophys. Res. Lett.* **34**, L22106, 10.1029/2007GL031504 (2007).
28. C. T. Russell, *Geophys. Res. Lett.* **16**, 1253 (1989).

29. We thank all those who contributed to the success of the first MESSENGER flyby of Mercury. Science discussions with S. A. Boardsen and M. Sarantos and data visualization and graphics support by C. Liebrecht and M. Marosy are gratefully acknowledged. The MESSENGER project is supported by the NASA Discovery Program under contracts NAS5-97271 to Johns Hopkins University Applied Physics Laboratory and NASW-00002 to the Carnegie Institution of Washington.

14 April 2008; accepted 3 June 2008
10.1126/science.1159040